A Comprehensive TCAD Approach for Assessing Electromigration Reliability of Modern Interconnects

Hajdin Ceric, Roberto Lacerda de Orio, Johann Cervenka, and Siegfried Selberherr, *Fellow, IEEE*

***Abstract*—The demanding task of assessing long-time interconnect reliability can only be achieved by combination of experimental and technology computer-aided design (TCAD) methods. The basis for a TCAD tool is a sophisticated physical model which takes into account the microstructural characteristics of copper. In this paper, a general electromigration model is presented with special focus on the influence of grain boundaries and mechanical stress. The possible calibration and usage scenarios of electromigration tools are discussed. The physical soundness of the model is proved by 3-D simulations of typical dual-damascene structures used in accelerated electromigration testing.**

***Index Terms*—Electromigration, interconnect, layout design, physical modeling, reliability, simulation.**

I. Introduction

ELECTROMIGRATION is the main reliability issue in modern integrated circuits, which can trigger system failure at some undefined future time. The phenomenon is particularly likely to afflict the thin tightly spaced interconnect lines of deep-submicrometer designs.

Because it first gained importance for microelectronics back-end technology, engineers, physicists, and material scientists have tried to understand and model electromigration. The necessity to reduce electromigration risk was huge from the very beginning, and with the introduction of new technologies, it is even more increasing.

Because the phenomenon does not manifest itself until a circuit has been operated for months, or even years, electromigration cannot be prevented by product testing.

Blech *et al.* [1]–[3] were one of the first to explain the origin of the electromigration phenomena. In their experiments, they discovered a critical product of interconnect line length and current density, below which no electromigration failure is observed. Kirchheim and Kaeber [4], [5] proposed a physically based model in which generation of stress in the grain boundaries during electromigration is caused by annihilation and generation of vacancies. Korhonen *et al.* [6] proposed another physics-based analytical model for mechanical stress evolution during electromigration in a confined metal line, which is described by a 1-D equation.

Manuscript received January 13, 2008; revised April 29, 2008. First published October 31, 2008; current version published March 6, 2009. This work was supported by the Austrian Science Fund under Project P18825-N14.

The authors are with the Institut für Mikroelektronik, Technische Universität Wien, 1040 Vienna, Austria.

Digital Object Identifier 10.1109/TDMR.2008.2000893

Experimental observations of void evolution in interconnect lines using *ex situ* and *in situ* transmission and scanning electron microscopy (SEM) have significantly improved our understanding of the various failure mechanisms in interconnect lines, for example [7]–[11].

An ultimate hope of integrated circuit designers today is to have a computer program which predicts the behavior of thin film metallizations under any imaginable condition. Contemporary integrated circuits are often designed using simple and conservative design rules to ensure that the resulting circuits meet reliability goals. This precaution leads to reduced performance for a given circuit and metallization technology.

The main challenge in electromigration modeling and simulation is the diversity of the relevant physical phenomena. Electromigration-induced material transport is also accompanied by material transport driven by the gradients of material concentration, mechanical stress, and temperature distribution. A comprehensive physics-based analysis of electromigration for modern copper interconnect lines serves as the basis for deriving sophisticated design rules which will ensure higher steadfastness of interconnects against electromigration.

Relaying of previous work, we present our model which reveals an improvement in two major points. First, there is a complete integration of mechanical stress phenomena in the connection with microstructural aspects in the classical multidriving force continuum model, and secondly, a newly developed finite-element-based scheme enables an efficient numerical solution of the 3-D formulation of the problem while the physical soundness is preserved. A satisfying assessment of electromigration reliability can only be achieved through combination of experimental methods and utilization of TCAD tools. Therefore, in this paper, we also discuss a possible usage scenario of TCAD tools in connection with results of accelerated interconnect tests.

II. TCAD Solutions for Electromigration

Competitive reliability targets of chip failure rates have been on the order of one per thousand throughout the anticipated lifetime in the field. The central problem of the interconnect design for reliability is the determination of the long-term interconnect behavior.

The TCAD analysis of the electromigration reliability of interconnect structures has to be carried out on at least two levels. The first level is without any doubt a physical one, which means

the application of most complete and comprehensive models to interconnect portions of moderate size. The restriction in size and complexity arises from the capacity of computers (memory, computational time) but has also a cause in numerical issues. The first level analysis is based on the simulation of the behavior of characteristic portions of the interconnect, which, known from experiments, represent a high electromigration risk. The goal of the analysis by simulation is to determine the time-to-failure (TTF) distribution for this specific interconnect part.

The second level analysis combines the results of the first level in order to assess the electromigration reliability of an entire chip. If the first level analysis $\mathrm{PDF}_k(t)$, $k = 1, \ldots, N$ (probability density function) provides a TTF distribution for each of N characteristic parts of the interconnect, the cumulative TTF distribution $\mathrm{CDF}(t)$ (cumulative distribution function) for the entire chip is [12]–[14]

$$\mathrm{CDF}(t) = 1 - \prod_{k=1}^{N} \left[1 - \int_0^t \mathrm{PDF}_k(t')dt' \right]. \tag{1}$$

Although there is no stated industry standard, competitive reliability targets of chip failure have been $\mathrm{CDF}(t) < 0.1\%$ for the time of $t = 10$ or $t = 15$ years.

III. Physically Based Modeling

Generally, the evolution of electromigration induced failure consists of two phases. In the first phase which we call the void nucleation phase, the interconnect materials undergo an inner transformation followed by the buildup of mechanical stress, which leads to the formation of an initial void. In this phase, no significant change in the interconnect resistance can be observed. This phase is followed by the void evolution phase in which the void can be observed on SEM and transmission electron microscopy pictures. The resistance change in this phase can still be hardly observable. The situation changes when a void wanders to a position inside the interconnect which the geometrical constellation causes that even a small void and its evolution induces a large resistance change. Another scenario of the rapid resistance change is when the local geometrical conditions enhance a rapid void growth.

The theoretical models of electromigration and accompanied driving forces of material transport have gone through a long evolution starting with early works of Blech *et al.* [1]–[3], over very substantial contributions of Mullins [15], Korhonen *et al.* [6], Lloyd *et al.* [16], [17], and Clement [18], to general contemporary models of Sarychev and Zhitnikov [19] and Sukharev [20].

A. Electrothermal Problem

Preceding the consideration of the electromigration model equations, an electrothermal problem has to be solved. The goal is to obtain an accurate temperature distribution. All diffusivities in the electromigration model are thermally activated and even a small error in the temperature calculation can lead to a substantial error in the vacancy concentration and stress calculation.

The global transient electrothermal behavior of the interconnect is described by the equation system [21]

$$\nabla \cdot (\gamma_T \nabla T) = c_p \rho_m \frac{\partial T}{\partial t} - p \tag{2}$$

$$p = \gamma_E \|\nabla \varphi\|^2 \tag{3}$$

$$\nabla \cdot (\gamma_E \nabla \varphi) = 0 \tag{4}$$

where γ_T represents the material specific thermal conductivity, γ_E is the electrical conductivity, p is the electrical power loss density, c_p is the specific heat, and ρ_m is the mass density. As solution, the temperature distribution in the interconnect, barrier, and passivation layers is obtained.

While dealing with the electrothermal model, special care must be taken in setting thermal boundary conditions. In order to consider the effect of Joule heating properly, a sufficiently big portion of dielectric surrounding the interconnect structure must be included in the simulation. A thermal reservoir, represented by a Dirichlet boundary condition in temperature, is then set on one side of the geometry with a direct contact only to the dielectric.

B. Bulk Vacancy Transport

The bulk vacancy transport is given by the following balance equation:

$$\frac{\partial C_v}{\partial t} = -\mathrm{div}\mathbf{J}_v \tag{5}$$

where $\mathbf{J}_v$ is the vacancy flux driven by electromigration ($\sim \nabla\varphi$), the gradients of the vacancy concentration (∇C_v), and the mechanical stress ($\nabla \mathrm{tr}(\bar{\bar{\sigma}})$)

$$\mathbf{J}_v = -\mathbf{D}^v \left(\frac{Z^* e}{k_B T} C_v \nabla\varphi + \nabla C_v + \frac{f\Omega}{3k_B T} C_v \nabla \mathrm{tr}(\bar{\bar{\sigma}}) \right). \tag{6}$$

Here, $k_B T$ is the thermal energy, $Z^* e$ is the effective valence, Ω is the volume of atom, and f is the vacancy to atom volume ratio. $\mathbf{D}^v$ is the tensorial vacancy diffusivity which is in stress-free state set as $D^v_{ij} = D_{\mathrm{bulk}}\delta_{ij}$, where D_{bulk} is the isotropic bulk diffusivity.

Divergences of the vacancy flux produce local strain [22]

$$\frac{\partial \varepsilon^v_{ij}}{\partial t} = \frac{1}{3}\Omega(1-f)\mathrm{div}\mathbf{J}_v\delta_{ij} \tag{7}$$

which is equilibrated by induced displacements in the copper bulk $\mathbf{u} = \mathbf{u}(u_1, u_2, u_3)$ according to the Lamé–Navier equations

$$\mu\Delta u_i + (\mu+\lambda)\frac{\partial}{\partial x_i}(\nabla \mathbf{u}) = B\frac{\partial \mathrm{tr}(\varepsilon^v)}{\partial x_i}, \qquad i = 1, 2, 3. \tag{8}$$

Here, λ and μ are the Lamé coefficients and $B = \lambda + 2\mu/3$. Generally, an elastic deformation of the metal is assumed

$$\sigma_{ij} = \sum_{ijkl} \mathbf{C}_{kl}\varepsilon_{kl} \tag{9}$$

with the small displacement approximation

$$\varepsilon_{ij} = \frac{1}{2}\left(\frac{\partial u_i}{\partial x_j} + \frac{\partial u_j}{\partial x_i}\right), \qquad i,j = 1,2,3. \tag{10}$$

C. Impact of Mechanical Strain on Electromigration

The choice of passivating film material and corresponding process technology causes tensile or compressive stress in the interface between the passivating film and the interconnect metal. Interfacial compressive stress diminishes electromigration along interfaces by reducing diffusivity [23]. However, numerous experimental observations have shown [17] that tensile stress in the interface increases the possibility of failure. Increased thickness and rigidity of the capping layer prevents relaxation of both thermal and electromigration-induced stress, which results in dielectric cracking and metal extrusion. The local stress state introduces an anisotropy of the diffusivity. The dependence of the tensorial diffusivity on the stress state is given by the following relationship [24]:

$$D_{ij}^{v} = \frac{\Gamma_0}{2}\sum_{k=1}^{12} x_i^k x_j^k \exp\left(-\frac{\vec{\varepsilon}_I^{\,k}\Omega(\mathbf{C}\vec{\varepsilon})}{k_B T}\right). \tag{11}$$

x_i^k is the ith component of the jump vector $\vec{r}^{\,k}$ for a site k, $\vec{\varepsilon}$ is the applied anisotropic strain, $\mathbf{C}$ is the elasticity, $\vec{\varepsilon}_I^{\,k}$ is the strain induced by a single vacancy in the jump direction defined by the unit vector $\vec{n}_k = \vec{r}^{\,k}/|\vec{r}^{\,k}|$, and Γ_0 is the vacancy-atom exchange rate. The basis for this model, the relationship (11), was first presented in the theory of Dederichs *et al.* [25]. We use (11) to model the capping-stress impact on the cumulative material transport given by (6).

For both capping and liner layer, the quality of adhesion is of crucial importance. The adhesion quality can be influenced by the choice of processes and materials; for example, the following combinations have been extensively investigated: Cu/TiW, Cu/SiO_2, TiW/Cu/TiW, W/Cu/TiW, and SiO_2/Cu/TiW [26]. Weak bonding between the copper and the capping layer not only enhances electromigration prior to void nucleation but also speeds up void evolution and growth. Observations showed that an epitaxylike (e.g., uninterrupted array of parallel lattice planes) transition between copper and capping strengthens the copper/capping bonding [27].

D. Grain Boundaries

The basis for the actual understanding of vacancy dynamics in the presence of grain boundaries is Fisher's model [28]. This model includes two mechanisms: vacancy diffusion in the grain boundary and material exchange between the grain boundary and grain bulk. During electromigration grain boundaries play an important role in stress relaxation. Therefore, Fisher's model alone cannot be sufficient for the complete description of grain boundary physics.

We consider the famous relationship given by Herring and Blech for a chemical potential on the material surfaces and grain boundaries [1], [29]

$$\mu_v^{\mathrm{gb}} = \mu_0 + \Omega\sigma_{nn} \tag{12}$$

as a basis for the extension of Fisher's grain boundary model. μ_0 is some chemical reference potential, $\sigma_{nn} = \vec{n}\cdot\bar{\bar{\sigma}}\cdot\vec{n}$, and $\vec{n}$ is the normal to the grain surface. This relationship is obtained by a careful equilibrium analysis of the material exchange between the grain bulk and the grain boundary [29]–[31].

In the case that the vacancy concentration varies along the grain boundary, we have to extend (12) with a concentration contribution

$$\mu_v^{\mathrm{gb}} = \mu_0 + \Omega\sigma_{nn} + k_B T \ln\left(\frac{C_v^{\mathrm{gb}}}{C_v^0}\right). \tag{13}$$

Assuming that, in equilibrium, $\mu_v^{\mathrm{gb}} = \mu_v = \mu_0$, it follows [32] that

$$C_v^{\mathrm{gb,eq}} = C_v^0 \exp\left(-\frac{\sigma_{nn}\Omega}{k_B T}\right). \tag{14}$$

The expression for the vacancy flux along a grain boundary is now

$$J_v^{\mathrm{gb}} = \frac{D_v^{\mathrm{gb}} C_v^{\mathrm{gb}}}{k_B T}\frac{\partial \mu_{\mathrm{gb}}}{\partial l} \tag{15}$$

where l is the distance along the grain boundary.

Fisher's expression for a vacancy diffusion inside the grain boundary is

$$\frac{\partial C_v^{\mathrm{gb}}}{\partial t} = -\frac{\partial J_v^{\mathrm{gb}}}{\partial l} - \frac{1}{\delta}\left(J_v^2 - J_v^1\right). \tag{16}$$

By taking J_v^2 and J_v^1 to be normal components of the fluxes from both sides of the grain boundary, the extension of the originally 2-D model to a 3-D situation is straightforward. The emission and absorption of the vacancies will be regulated by the fluxes J_v^2 and J_v^1, and at the same time, both of these fluxes will be regulated by stress (σ_{nn}).

The chemical potential of the vacancies in the bulk is given by [33]

$$\mu_v = \mu_0 + k_B T \ln\left(\frac{C_v}{C_v^0}\right) + \frac{1}{3} f\Omega \mathrm{tr}(\bar{\bar{\sigma}}). \tag{17}$$

In the continuum modeling approach, the grain boundary as a vacancy transport medium is defined by the chemical potential (13). This chemical potential is constant through the grain boundary thickness and equal to the bulk chemical potential on the interfaces to the bulk regions, e.g., $\mu_v^1(-\delta/2) = \mu_v^2(+\delta/2) = \mu_{\mathrm{gb}}$, Fig. 1.

The vacancy fluxes on both sides of the grain boundary are given by

$$J_v^1 = \frac{D_v C_v}{k_B T}\nabla\mu_v^1 \tag{18}$$

$$J_v^2 = \frac{D_v C_v}{k_B T}\nabla\mu_v^2. \tag{19}$$

The difference $J_v^2 - J_v^1$ is an actual loss (gain) of vacancies which is localized at the thin slice which represents the grain

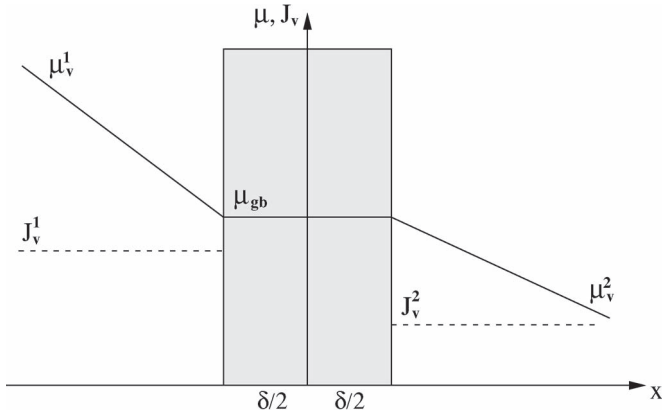

Fig. 1. Grain boundary according to Fisher's model and Herring's relationship.

boundary (in continuum modeling). The recombination rate can now be approximated as

$$G = \frac{\partial C_v}{\partial t} = -\mathrm{div} J_v \approx -\frac{J_v^2 - J_v^1}{\delta}. \tag{20}$$

The combination of Herring's and Fisher's modeling approaches enables a certain insight in the vacancy dynamics in the presence of grain boundaries; however, for numerical implementation, such a method is rather inconvenient.

We introduce a new model, where a grain boundary is treated as a separate medium with the capability of absorbing and releasing vacancies. We assume that vacancies are trapped from both neighboring grains with the trapping rate ω_T and released to these grains with a release rate ω_R. An equilibrium relationship structurally similar to (14) is obtained

$$C_v^{\mathrm{eq}} = C_v^0 \exp\left(-\frac{p\Omega}{k_B T}\right) \tag{21}$$

where $p = -\mathrm{tr}(\bar{\bar{\sigma}})/3$ is the hydrostatic stress.

The vacancy concentration from both sides of the grain boundary is denoted as $C_{v,1}$ and $C_{v,2}$, and correspondingly, fluxes are calculated as

$$J_{v,1} = \omega_T \left(C_v^{\mathrm{eq}} - C_v^{\mathrm{im}}\right) C_v^1 - \omega_R C_v^{\mathrm{im}} \tag{22}$$

$$-J_{v,2} = \omega_T \left(C_v^{\mathrm{eq}} - C_v^{\mathrm{im}}\right) C_v^2 - \omega_R C_v^{\mathrm{im}}. \tag{23}$$

C_v^{im} is the concentration of immobile vacancies which are trapped inside the grain boundary. Instead of (20), the following relationship can be stated:

$$\frac{\partial C_v^{\mathrm{im}}}{\partial t} = \frac{J_{v,1} - J_{v,2}}{\delta} = -\left(\frac{\partial C_{v,1}}{\partial t} + \frac{\partial C_{v,2}}{\partial t}\right). \tag{24}$$

Taking (22) and (23) into account, we obtain the final relationship

$$-G = \frac{\partial C_v^{\mathrm{im}}}{\partial t} = \frac{1}{\tau}\left(C_v^{\mathrm{eq}} - C_v^{\mathrm{im}}\left(1 - \frac{2\omega_R}{\omega_T(C_{v,1} + C_{v,2})}\right)\right) \tag{25}$$

with

$$\frac{1}{\tau} = \frac{\omega_T(C_{v,1} + C_{v,2})}{\delta}. \tag{26}$$

In order to include the effect of the grain boundary as a vacancy sink (source) into the bulk vacancy transport model (Section III-B), the recombination term G has to be included in (5) and (7). We obtain [22]

$$\frac{\partial C_v}{\partial t} = -\mathrm{div}\mathbf{J}_v + G \tag{27}$$

$$\frac{\partial \varepsilon_{ij}^v}{\partial t} = \frac{1}{3}\Omega\left((1-f)\mathrm{div}\mathbf{J}_v + fG\right)\delta_{ij}. \tag{28}$$

Equations (27) and (28) are solved inside the grain boundary. The flux $\mathbf{J}_v$ is again calculated according to (6), but this time (stress-free state), the diffusivity tensor is set as $D_{ij}^v = D_{\mathrm{gb}}\delta_{ij}$. D_{gb} is the grain boundary diffusivity which is several orders of magnitude higher than D_{bulk}.

The full description of the atomic mechanisms of vacancy generation and annihilation in grain boundaries goes beyond the capability of continuum modeling and can only be obtained by molecular dynamics methods [34].

E. Void Nucleation Condition

From the early days of electromigration modeling for the void nucleation condition, viz., transition from the first to the second phase of failure evolution, the following two conditions are used: 1) void nucleation after reaching a vacancy (atom) concentration threshold [35], [36] and 2) void nucleation after reaching a tensile stress threshold [37], [38].

However, a careful investigation based on classical nucleation theory has shown that these nucleation conditions from a thermodynamic point of view cannot be justified.

The classical nucleation theory studies the situation where, in a strained single-phase material, a droplet of the second phase embryo is produced by spontaneous fluctuations which overcome the barrier energy ΔF^* given by [39]

$$\Delta F^* = \frac{48\pi\gamma_m^3}{\left(\mathrm{tr}(\bar{\bar{\sigma}})\right)^2} \tag{29}$$

for spherical embryos. Here, γ_m is the surface free energy and σ is the applied stress field. When we assume a rather high hydrostatic pressure of 1 GPa [40] and take the surface free energy of copper 1.72 J/m^2 [41], we obtain an energy barrier of 133 eV. The number of critical embryos per unit volume is given by [39]

$$Z^* = \frac{1}{\Omega n^*}\left(\frac{\Delta F^*}{3\pi k_B T}\right)^{1/2} e^{-\frac{\Delta F^*}{k_B T}}. \tag{30}$$

Critical embryos are spontaneously formed by the condensation of vacancies in stressed copper. However, the condensation process is reversible, and in most cases, the embryos completely dissolve in the surrounding lattice. The situation changes when a critical embryo starts to accept additional free vacancies.

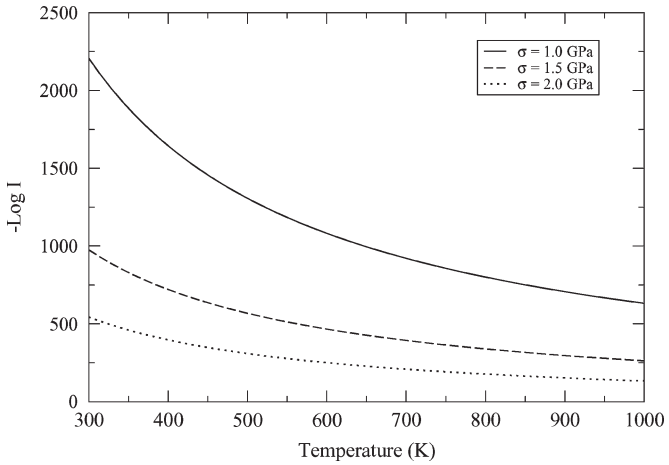

Fig. 2. Nucleation rate dependence on hydrostatic stress and temperature. Even a very high temperature cannot significantly increase the nucleation rate.

In such a case, the irreversible transition to an initial void is imminent [39]. The nucleation rate is then calculated as

$$I = \nu e^{-\frac{U_D}{k_B T}} Z^* n_s^* \tag{31}$$

where n_s^* is the number of vacancies in the matrix at the surface of the critical embryo. The calculated nucleation rate in the metal bulk is $I \sim 10^{-1396}$ m^{-3}s^{-1}. The temperature/stress dependence of the nucleation rate is shown in Fig. 2. Similar values can be obtained for nucleation at the interconnect sidewall, grain boundaries, and sidewall/grain boundary intersection. This means that void nucleation by vacancy condensation for both, accelerated test conditions and realistic use conditions, is not possible.

An analysis carried out by Flinn [42] gave a new framework for the understanding of void nucleation. The author considers a circular patch on the interface between copper and the capping layer with virtually no adhesion. Such an entity can actually be caused by a surface defect or contamination [43]. As the stress in the line increases, the free metal surface is driven to adopt an equilibrium, half-spherical shape, and a void embryo forms. The stress threshold given by Clemens *et al.* [44] and Glaixner *et al.* [40] is

$$\sigma_{\rm th} = \frac{2\gamma_m \sin\theta_c}{R_p}. \tag{32}$$

R_p is the radius of the adhesion-free patch, and θ_c is the critical angle. For stresses $\sigma < \sigma_{\rm th}$, an energy barrier exists between the embryo and a stable-growing void. If the stress is above the threshold value $(\sigma > \sigma_{\rm th})$, the free energy monotonically decreases with void volume and the energy barrier vanishes. If we now assume the adhesion free patch with a radius of 10 nm (about 20 atoms) and $\theta_c = \pi/2$, we obtain $\sigma_{\rm th} \approx 344$ MPa. In modern interconnects, this stress level can already be reached by thermal stress [45].

IV. Some Remarks on Modeling the Void Evolution Phase

When the stress level defined by (32) is reached at some interfacial spots where a flaw can be assumed, the failure development enters the next phase and a different modeling Ansatz must be applied. Here, we have an evolving void surface shaped by two dynamic forces: the chemical potential gradient and the electron wind. Including both contributions, electromigration and chemical potential-driven surface diffusion, gives the total surface vacancy flux $\mathbf{J_s} = J_s\mathbf{t}$, where $\mathbf{t}$ is the unit vector tangential to the void surface [46], [47]

$$J_s = -D_s\left(eZ^*E_s + \Omega\nabla_s\left(\frac{\sigma:\varepsilon}{2} - \gamma_s\kappa\right)\right). \tag{33}$$

$E_s \equiv \mathbf{E_s}\cdot t$ is the local component of the electric field tangential to the void surface, ∇_s is the surface gradient operator, 1/2 $(\sigma:\varepsilon)$ is the strain energy density of the material adjacent to the void surface, and κ is the curvature of the void surface. D_s is given by an Arrhenius law

$$D_s = \frac{D_0\delta_s}{k_B T}\exp\left(-\frac{Q_s}{k_B T}\right). \tag{34}$$

δ_s is the thickness of the diffusion layer, Q_s is the activation energy for the surface diffusion, and D_0 is the preexponential coefficient for mass diffusion.

Numerical tracking of the surface is necessary, because it fully determines the failure dynamics. The shape of the voids together with local geometry conditions cause changes in the interconnect resistance and the speed of the void growth. Thus, the migration direction is strongly influenced by the shape of a void.

The 3-D algorithms for simulation of the void surface evolution are computationally very demanding, and currently no satisfactory solution exists. A simplified version of the 2-D successfully applied diffuse interface model [47], [48] maybe a promising candidate for a solution.

V. Numerical Aspects

A. Numerical Algorithm of the Compound Problem

The mathematical description of the electromigration model consists of six partial differential equations which are solved for the scalar fields $V(\vec{r})$, $T(\vec{r})$, $C_v(\vec{r})$, and the vector displacement field $\vec{u}(\vec{r})$. Because of the nonlinear dependence of electrical and thermal conductivies on temperature and the nonlinear dependence of the diffusion coefficients on temperature and strain, the complete equation system is nonlinear. The method of choice for the given problem is the finite-element method (FEM), because of its generality and due to the fact that it is a well-investigated approach for mechanical problems.

A solving algorithm is implemented in our in-house finite-element code. Each model is handled according to the unique priority list, starting with the electrothermal equations (2) and (3), over the material transport equations (6), (5), to the mechanical model (8)–(10), and the equations describing the influence of the local vacancy dynamics on strain [(25), (27) and (28)]. The calculated attributes are transfered from the model of higher priority to the model of lower priority, cf. Fig. 3.

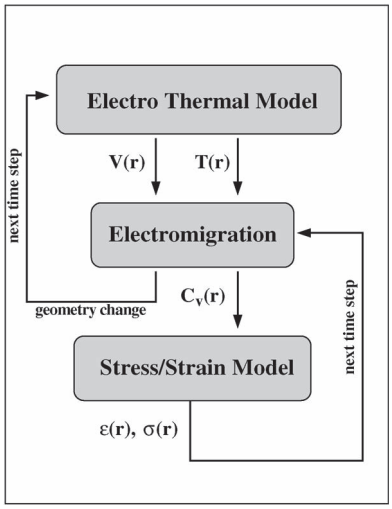

Fig. 3. Complete solving procedure. In each time step, the electrothermal, mechanical, and electromigration problems are solved.

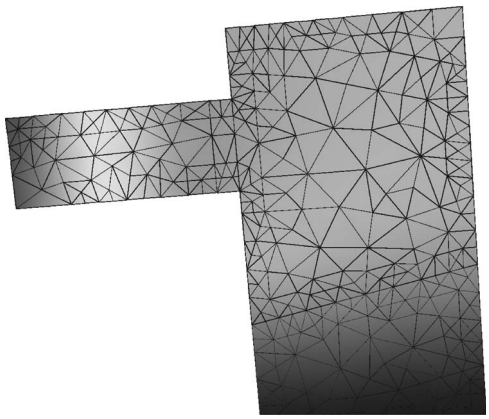

Fig. 4. Grain boundary plane is surrounded at both sides with slices spatially discretized with fine tetrahedra. In these slices, high grain boundary diffusivities are set, and at the same time, the Rosenberg–Ohring term is activated.

B. Numerical Realization of the Grain Boundary Model

Grain boundaries, and generally, every interface of the problem geometry have to be supplied with an appropriately fine FEM mesh. This is necessary in order to provide sufficient resolution for the local dynamics described with the relationships (25), (27) and (28), cf. Fig. 4.

VI. Usage Scenario for TCAD Tools

Simulation can be used for the extrapolation of long-time interconnect behavior on the basis of results of accelerated electromigration tests. This capability goes clearly beyond an extrapolation by standard statistical methods which rely on Black's equation and extrapolate a TTF for a single interconnect structure. The usage of TCAD tools enables a prediction of the behavior for structures which are obtained by the variation of geometrical properties and operating conditions of a previously used initial test structure.

The assumed scenario for the application of an electromigration reliability TCAD tool is the following.

- Model Calibration. For this purpose, we use one layout and many test units. At the end of calibration, all parameters of the model are fixed. During this process, different microstructures are considered and simulation parameters are varied with the goal to reproduce experimental failure time statistics, Fig. 5.
- Model Application. The calibrated model is used for simulation. The simulation extrapolates the behavior of the interconnect under real life conditions.

For a given interconnect layout and monocrystalline material, simulation will provide a unique TTF. All impact factors, e.g., geometry of the layout, bulk diffusivity, interface diffusivity, and mechanical properties, are deterministic, and therefore, TTF is deterministic. However, the situation changes when the interconnect possesses a microstructure. The microstructure has a significant impact on electromigration, because it introduces a diversity of possible electromigration paths and local mechanical properties (the Young modulus and Poisson factor depend on the crystal orientation in each grain). However, the microstructure itself cannot be completely controlled by a process technology. In other words, the position of grain boundaries, angles in which they meet the interfaces, etc., cannot be designed; the process itself determines only statistics of grain sizes and textures.

If we extract statistical properties of the microstructure obtained by a specific process used for producing a test structure and use these properties to design an input for simulation tools, the resulting TTF distribution from the simulation with these inputs has to fit the experimental distribution. If this is not the case, the configurable parameters of the model have to be varied, until the simulated TTF distribution fits the experimental one. When a reasonable agreement between the experimentally determined TTF distribution and the simulated TTF distribution is reached, the TCAD tool is considered as calibrated and can be used for electromigration reliability assessment under realistic operating conditions.

VII. Simulative Studies and Discussion

A. Transition in Equilibrium

Once the convergence and stability of a numerical algorithm is tested, it is necessary to investigate the physical soundness of the implemented numerical model. For this purpose, we chose a simple 3-D geometry. When an electric potential is applied, the system is forced to migrate into a new stable state. From the thermodynamic point of view, the system tries to reach a new minimum of overall free energy and the direction in which the system moves is determined by gradients of chemical potentials. In our case, the system undergoes an inner transformation due to electromigration and stressmigration. Eventually, the system reaches an equilibrium which is characterized by stable constant peak values of vacancy concentration and hydrostatic stress. In Fig. 6, the simulation result for the case of simple rectangular monocrystalline copper with 10-μm length is shown. The temperature is 473 K, and the current density is 4 MA/cm^2. Under these conditions, the equilibrium of both tensile and compressive stress is reached after 10 h. As expected, the peak values of tensile stress and vacancy concentration occur at the cathode end of the interconnect.

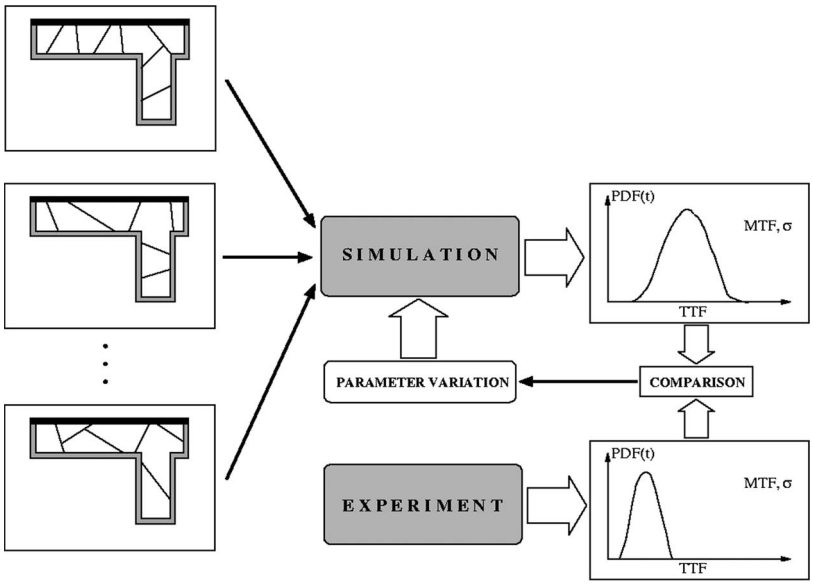

Fig. 5. Electromigration model calibration using a multitude of microstructural inputs.

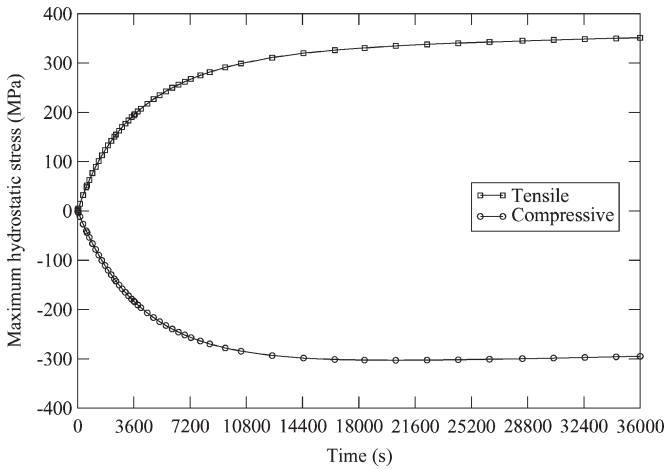

Fig. 6. Tensile and compressive stress behavior for a case of monocrystaline copper.

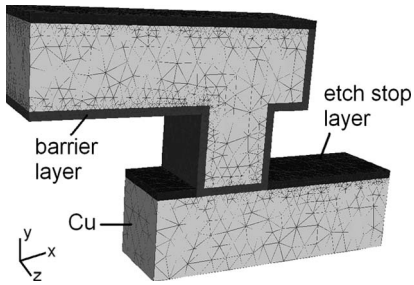

Fig. 7. Interconnect via geometry.

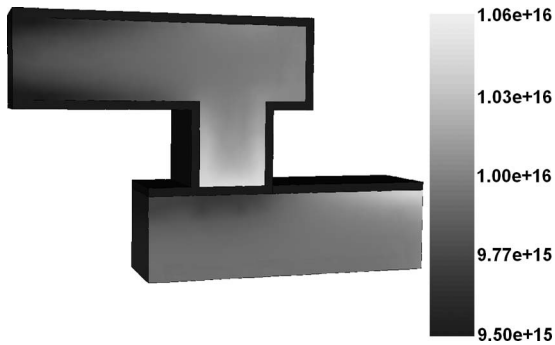

Fig. 8. Vacancy concentration for the interconnect without strains (units in per cubic centimeter). The higher vacancy concentration on the interface between the bottom copper line and the etch stop layer occurs due to the increased interfacial diffusion coefficient.

B. Residual Strain Dependent Electromigration

In structures produced by dual-damascene technology, residual stresses remain. The causes of these stresses are not only a thermal mismatch during cooling down from deposition to room temperature, but also microstructural evolution during and after deposition. The presence of the residual stresses induces a deformation of the copper crystal and the anisotropy of electromigration. Here, we extend the continuum electromigration according to the discussion presented in Section III-C.

The interconnect geometry analyzed by fully 3-D simulation is shown in Fig. 7. The interconnect line and via have a cross section of 0.2×0.2 μm^2, and the Tantalum barrier and etch stop layers have a thickness of 20 nm. Initially considering that the interconnect is free of strains, we obtain the vacancy distribution as shown in Fig. 8, with 10^{16} cm^{-3} used as the initial vacancy concentration for copper [6]. As expected, the vacancies concentrate "downstream," mainly in the via region, where the copper meets the barrier layer, with a small increase above the initial concentration. No change is observed in the vacancy distribution until strains on the order of 0.5%–1% are used. With $\epsilon_{xx} = 0.010$, $\epsilon_{yy} = 0.005$, and $\epsilon_{zz} = 0.001$, we have verified a very small increase in the vacancy concentration on the bottom of the via, as shown in Fig. 9. In this case, we have determined the off-diagonal components of the diffusivity tensor to be about 18% of the diagonal ones. Considering $\epsilon_{xx} = 0.008$, $\epsilon_{yy} = 0.015$, and $\epsilon_{zz} = 0.003$, the distribution of vacancies is significantly altered, although the change in the concentration values is still small, as Fig. 10 shows. These higher strains increased the off-diagonal diffusion coefficients to approximately 30% of the diagonal values. In conclusion, we have shown that

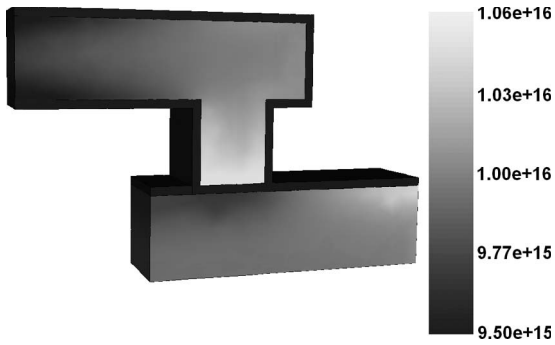

Fig. 9. Vacancy concentration for strains $\epsilon_{xx} = 0.010$, $\epsilon_{yy} = 0.005$, and $\epsilon_{zz} = 0.001$ (units in per cubic centimeter).

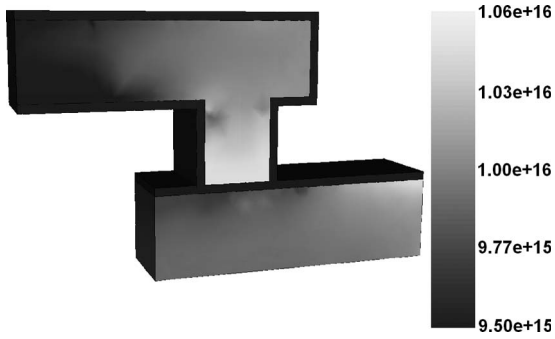

Fig. 10. Vacancy concentration for strains $\epsilon_{xx} = 0.008$, $\epsilon_{yy} = 0.015$, and $\epsilon_{zz} = 0.003$ (units in per cubic centimeter).

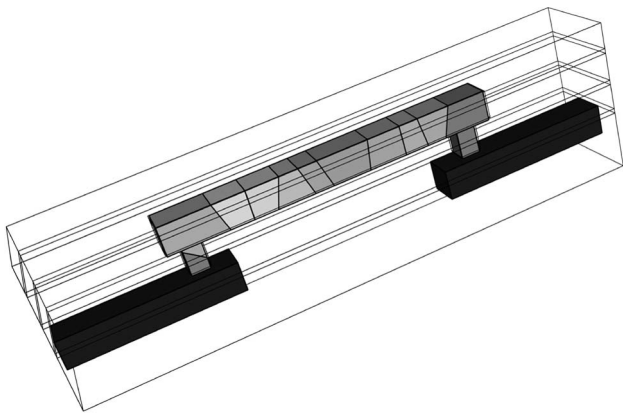

Fig. 11. Three-dimensional dual-damascene structure with polycrystalline copper metallization.

high strains and, consequently, stresses can lead to significant anisotropy of material transport in an interconnect line under electromigration stress. This effect must be taken into account for a rigorous analysis of the electromigration problem.

C. Electromigration in Multigrain Copper

We have applied our model to the interconnect layout which has been extensively used for accelerated electromigration tests [49]. This layout is typical for dual-damascene 0.18-μm technologies. The copper microstructure (Fig. 11) is set according to the results of electron backscatter diffraction measurements [50].

The peak values of stress and the vacancy concentration values are extracted from three extraction cylinders (C1, C2, and C3), which are shown in Fig. 12(a). The solution of the electrothermal problem sets the operating conditions for electromigration simulation. The applied mechanical, thermal, and electrical boundary conditions are shown in Fig. 12(b). Temperature T_0 is set on constant 673 K, and the voltage is $V_0 = 10$ mV. The obtained average current density is 10 MA/cm^2. Due to the geometry of the problem and the applied boundary conditions, the temperature is only slightly changed by Joule heating.

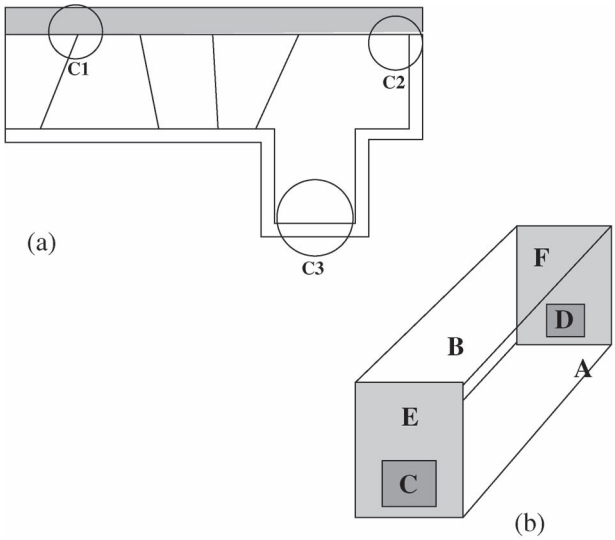

Fig. 12. (a) Peak values for hydrostatic stress and vacancy concentration values are extracted from cylinders C1, C2, and C3. (b) Applied boundary conditions. (A, B) Fixed temperature $T_0 = 673$. (C, D) Voltage $V_0 = 10$ mV, upstream electromigration from C3 to C1. (E, F) Mechanically fixed.

The vacancy release rate ω_R and vacancy trapping rate ω_T are chosen in such a way that, during simulation, following conditions are fulfilled:

$$\frac{2\omega_R}{\omega_T(C_{v,1} + C_{v,2})} \ll 1 \tag{35}$$

and

$$1\ \text{s} < \tau = \frac{\delta}{\omega_T(C_{v,1} + C_{v,2})} < 2\ \text{s}. \tag{36}$$

With these conditions, the model for immobile vacancies (22)–(26) behaves analogously to a classical Rosenberg–Ohring term [51], which was already successfully applied in [52] where $\tau = 1$ and $\tau = 2$ s are used.

In dual-damascene copper technologies, interfaces to capping (etch-stop) layers are recognized as the fastest material transport paths for standard capping dielectrics SiN_x [49]. Experimental investigations have shown that, for such cappings, critical voids are formed at the top corner of the cathode edge of metal line [52]. In order to properly include the effect of fast diffusivity paths, grain boundary, barrier, and capping layer diffusivities are set as $10^2 D_{\text{bulk}}$, $10^2 D_{\text{bulk}}$, and $10^5 D_{\text{bulk}}$, respectively. The applied bulk diffusivity value is [52]

$$D_{\text{bulk}} = 0.52 \exp\left(-\frac{1.1\ \text{eV}}{k_B T}\right) \frac{\text{cm}^2}{\text{s}}. \tag{37}$$

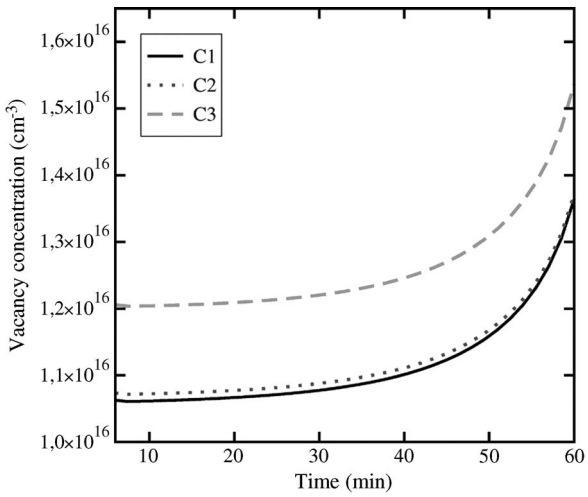

Fig. 13. Time evolution of vacancy concentration at three characteristic spots of the via.

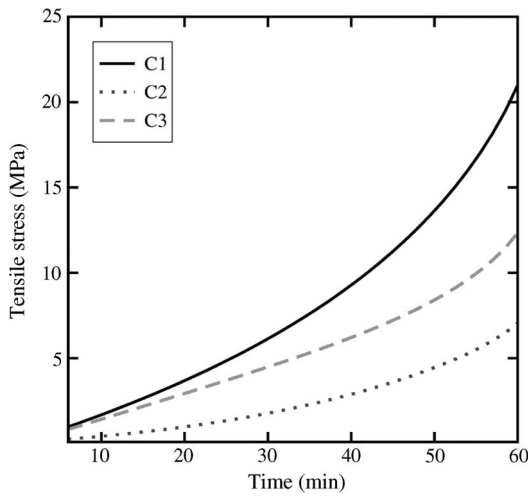

Fig. 14. Time evolution of tensile hydrostatic stress at three characteristic spots of the via.

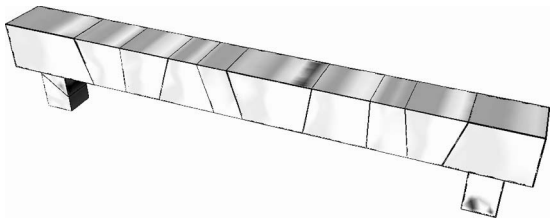

Fig. 15. Peak tensile stress tensor component distribution. Red-colored areas mark peak tensile stress.

As we may conclude from Section III-E, for possible void nucleation, we must have high tensile stress and a local interface defect. Therefore, the primary goal of our investigation is to determine the sites, where high stresses arise. For this purpose, we monitor the hydrostatic stress development in three value-extraction cylinders placed at the triple point next to cathode end of the via (C1), at the portion of the capping layer which lays directly above the via bottom (C2), and at the via bottom itself (C3), cf. Fig. 12(a).

Until approximately 10 min, the peak tensile stress and the vacancy concentration exhibit nearly exponential growth. After this phase, the peak vacancy concentration increases very slightly and the peak tensile stress grows linearly. Such a behavior was already observed and studied by Kirchheim [5], where it is called quasi-steady state. After the quasi-steady state, a rapid growth of stress and vacancy concentration takes place. In Fig. 13, a representative excerpt of the vacancy dynamics is given. Here, the transition from the quasi-steady state to the phase of rapid growth occurs after approximately 40 min.

Due to the geometry layout, the highest vacancy concentration always develops at the bottom of the cathode end of the via (C3). The peak vacancy concentration on the sites C1 and C2 develops approximately in the same way, but the site of highest stress (C1) does not coincide with the site of highest vacancy concentration (C3) (Fig. 14). The connection between tensile stress and local vacancy concentration is defined through relationship (28) and overall mechanical equilibrium (8). The local stress behavior does not depend only on the local vacancy concentration but also on mechanical conditions in the neighboring areas.

As observed in experiments [49] carried out under similar operating conditions like in our simulations, we have the first void nucleation after less than 2 h. According to our result, we have, at this time, already rapid stress growth and a stress level of about 70 MPa at the triple point C1 (Fig. 12(a) and Fig. 15).

It is obvious that a defect site is necessary for void nucleation, and the coincidence of high vacancy concentration and high tensile stress regions with triple points indicates that triple points are natural locations of weak adhesion. This assumption was also expressed in the discussion of results of accelerated tests published in [49] and [50].

The scenario of weak triple points in combination with a stress threshold would allow multiple void nucleations in the short time interval as it has actually already been observed [49]. These voids can migrate along the copper/capping layer interface, from one triple point to another, and stop at the corners above the via. Here, further void growth takes place, eventually resulting in a critical decrease in the effective interconnect cross section leading to failure.

VIII. Conclusion

A comprehensive electromigration model is presented as a basis for a 3-D simulation tool. The influence of residual and electromigration-induced strains on material transport is discussed, and an earlier electromigration model is extended by the introduction of tensorial self-diffusivity. An overview and a discussion of a grain boundary physics is provided, whereas a special focus was put on the stress influence on grain boundaries. A rigorous analysis of void nucleation conditions is given and possible consequences for simulation are discussed. The physical soundness of the extended electromigration model is verified with several simulation examples. The simulated dynamics of early failure development is in good agreement with experimental observations. The role of triple points for void nucleation is discussed on the basis of simulation and corresponding experimental results. A concept for usage of TCAD tools in combination with experimental tests is presented.

REFERENCES

[1] I. A. Blech and C. Herring, "Stress generation by electromigration," *Appl. Phys. Lett.*, vol. 29, no. 3, pp. 131–133, Aug. 1976.

[2] I. A. Blech, "Electromigration in thin aluminum films on titanium nitride," *J. Appl. Phys.*, vol. 47, no. 4, pp. 1203–1208, Apr. 1976.

[3] I. A. Blech and K. L. Tai, "Measurement of stress gradients generated by electromigration," *Appl. Phys. Lett*, vol. 30, no. 8, pp. 387–389, Apr. 1977.

[4] R. Kirchheim and U. Kaeber, "Atomistic and computer modeling of metallization failure of integrated circuits by electromigration," *J. Appl. Phys.*, vol. 70, no. 1, pp. 172–181, Jul. 1991.

[5] R. Kirchheim, "Stress and electromigration in Al-lines of integrated circuits," *Acta Metall. Mater.*, vol. 40, no. 2, pp. 309–323, 1992.

[6] M. A. Korhonen, P. Borgesen, K. N. Tu, and C. Y. Li, "Stress evolution due to electromigration in confined metal lines," *J. Appl. Phys.*, vol. 73, no. 8, pp. 3790–3799, Apr. 1993.

[7] E. Arzt, O. Kraft, W. D. Nix, and J. E. Sanchez, "Electromigration failure by shape change of voids in bamboo lines," *J. Appl. Phys.*, vol. 76, no. 3, pp. 1563–1571, Aug. 1994.

[8] M. A. Meyer, M. Herrmann, E. Langer, and E. Zschech, "*In Situ* SEM observation of electromigration phenomena in fully embedded copper interconnect structures," *Microelectron. Eng.*, vol. 64, no. 1–4, pp. 375–382, 2002.

[9] A. S. Oates, "Electromigration failure of contacts and vias in sub-micron integrated circuit metallisations," *Microelectron. Reliab.*, vol. 36, no. 7/8, pp. 925–953, Jul./Aug. 1996.

[10] C. L. Gan and F. Wei, "Contrasting failure characteristics of different levels of Cu dual-damascene metallization," in *Proc. 12th Int. Symp. Phys. Failure Anal. Integr. Circuits*, 2002, pp. 124–128.

[11] B. H. Jo and R. W. Vook, "In-Situ ultra-high vacuum studies of electromigration in copper films," *Thin Solids Films*, vol. 262, no. 1, pp. 129–134, Jun. 1995.

[12] A. H. Fischer, A. Abel, M. Lepper, A. E. Zitzelsberger, and A. von Glasow, "Experimental data and statistical models for bimodal EM failures," in *Proc. 38th Annu. IEEE Int. Rel. Phys. Symp.*, 2000, pp. 359–363.

[13] L. J. Bain and M. Engelhardt, *Statistical Analysis of Reliability and Life-Testing Models*. New York: Marcel Dekker, 1991.

[14] A. von Glasow, "Zuverlässigkeitsaspekte von Kupfermetallisierungen in Integrierten Schaltungen," Ph.D. dissertation, Technische Universität München, Munich, Germany, 2005.

[15] W. W. Mullins, "Mass transport at interfaces in single component systems," *Metall. Mater. Trans. A (USA)*, vol. 26, no. 8, pp. 1917–1929, Aug. 1995.

[16] J. Lloyd and E. Arzt, "A simple model for stress voiding in passivated thin film conductors," in *Proc. Symp. Mater. Rel. Microelectron. II*, 1992, vol. 265, pp. 45–57.

[17] J. Lloyd and J. J. Clement, "Electromigration in copper conductors," *Thin Solid Films*, vol. 262, no. 1, pp. 135–141, Jun. 1995.

[18] J. J. Clement, "Electromigration modeling for integrated circuit interconnect reliability analysis," *IEEE Trans. Device Mater. Rel.*, vol. 1, no. 1, pp. 33–42, May. 2001.

[19] M. E. Sarychev and Y. V. Zhitnikov, "General model for mechanical stress evolution during electromigration," *J. Appl. Phys.*, vol. 86, no. 6, pp. 3068–3075, Sep. 1999.

[20] V. Sukharev, "Simulation of microstructure influence on EM-induced degradation in Cu interconnects," in *Proc. 8th Int. Workshop AIP Conf. Stress-Induced Phenom. Metallization*, 2005, vol. 817, pp. 244–253.

[21] R. Sabelka and S. Selberherr, "SAP—A program package for three-dimensional interconnect simulation," in *Proc. Interconnect Technol. Conf.*, 1998, pp. 250–252.

[22] H. Ceric, R. Heinzl, C. Hollauer, T. Grasser, and S. Selberherr, "Microstructure and stress aspects of electromigration modeling," in *Proc. AIP Stress-Induced Phenom. Metallization*, 2006, pp. 262–268.

[23] J. Lloyd and K. P. Rodbell, "Reliability," in *Handbook of Semiconductor Interconnection Technology*, G. C. Schwartz and K. V. Srikrishnan, Eds. New York: Elsevier, 2006, pp. 471–520.

[24] R. L. de Orio, H. Ceric, and S. Selberherr, "Effect of strains on electromigration material transport in copper interconnect structures under electromigration stress," *J. Comput. Electron.* [Online]. Available: http://www.springerlink.com/content/6142u5642220078k/

[25] P. H. Dederichs and K. Schroeder, "Anisotropic diffusion in stress fields," *Phys. Rev. B, Condens Matter*, vol. 17, no. 6, pp. 2524–2536, Mar. 1978.

[26] H. Kang, I. Asano, C. Ryu, and S. Wong, "Grain structure and electromigration properties of CVD CU metallization," in *Proc. 10th Int. VLSI Multilevel Interconnection Conf.*, 1993, pp. 223–229.

[27] E. Zschech, M. A. Meyer, S. G. Mhaisalkar, A. V. Vairagar, A. Krishnamoorthy, H. J. Engelmanna, and V. Sukharev, "Effect of interface modification on EM-induced degradation mechanisms in copper interconnects," in *Proc. ICMAT Conf.*, 2005, vol. 504, no. 1–2, pp. 279–283.

[28] J. C. Fisher, "Calculation of diffusion penetration curves for surface and grain boundary diffusion," *J. Appl. Phys.*, vol. 22, no. 1, pp. 74–77, Jan. 1951.

[29] C. Herring, "Diffusional viscosity of polycrystalline solid," *J. Appl. Phys.*, vol. 21, no. 5, pp. 437–445, May 1950.

[30] C. Herring, "Surface tension as a motivation for sintering," in *Physics of Powder Metallurgy*, W. E. Kingston, Ed. New York: McGraw-Hill, 1951, pp. 143–179.

[31] C. Herring, "The use of classical macroscopic concepts in surface energy problems," in *Structure and Properties of Solid Surfaces*, R. Gomer and S. Smith, Eds. Chicago, IL: Univ. Chicago, 1952, pp. 5–81.

[32] R. W. Balluffi and A. V. Granato, "Dislocations, vacancies and interstitials," in *Dislocation in Solids*, F. N. R. Nabarro, Ed. Amsterdam, The Netherlands: North-Holland, 1979, pp. 1–133.

[33] F. C. Larche and J. Cahn, "The Interactions of composition and stress in cystalline solids," *Acta metall.*, vol. 33, no. 3, pp. 331–357, 1985.

[34] M. R. Sorensen, Y. Mishin, and A. F. Voter, "Diffusion mechanisms in Cu grain boundaries," *Phys. Rev. B, Condens. Matter*, vol. 62, no. 6, pp. 3658–3673, Aug. 2000.

[35] O. Kraft and E. Arzt, "Current density and line width effects in electromigration: A new damage-based lifetime model," *Acta Mater.*, vol. 46, no. 11, pp. 3733–3743, Jul. 1998.

[36] V. Sukharev, R. Choudhury, and C. W. Park, "Physically-based simulation of the early and long-term failures in the copper dual damascene interconnect," in *Proc. IEEE Int. Rel. Workshop Final Rep.*, 2003, pp. 80–85.

[37] C. L. Gan, C. V. Thompson, K. L. Pey, W. K. Choi, H. L. Tay, B. Yu, and M. K. Radhakrishnan, "Effect of current direction on the lifetime of different levels of Cu dual-damascene metallization," *Appl. Phys. Lett*, vol. 79, no. 27, pp. 4592–4594, Dec. 2001.

[38] J. T. Trattles, A. G. O'Neill, and B. C. Mecrow, "Computer simulation of electromigration in thin-film metal conductors," *J. Appl. Phys.*, vol. 75, no. 12, pp. 7799–7804, Jun. 1994.

[39] J. W. Christian, *The Theory of Transformations in Metals and Alloys, PART I*. New York: Pergamon, 2002.

[40] R. J. Gleixner, B. M. Clemens, and W. D. Nix, "Void nucleation in passivated interconnect lines: Effects of site geometries, interfaces, and interface flaws," *J. Mater. Res.*, vol. 12, no. 8, pp. 2081–2090, Aug. 1997.

[41] D. A. Porter and K. E. Easterling, *Phase Transformations in Metals and Alloys*. Cheltenham, U.K.: Stanley Thornes Publishers Ltd, 2000.

[42] P. A. Flinn, "Mechanical stress in VLSI interconnections: Origins, effects, measurement, and modeling," *MRS Bull.*, vol. 20, no. 11, pp. 70–73, Nov. 1995.

[43] E. Zschech, H.-J. Engelmann, M. Meyer, V. Kahlert, A. V. Vairagar, S. G. Mhaisalkar, A. Krishnamoorthy, M. Yan, K. N. Tu, and V. Sukharev, "Effect of interface strength on electromigration-induced inlaid copper interconnect degradation: Experiment and simulation," *Zeitschrift fur Metallkünde*, vol. 96, no. 9, pp. 966–971, 2005.

[44] B. M. Clemens, W. D. Nix, and R. J. Gleixner, "Void nucleation on a contaminated patch," *J. Mater. Res.*, vol. 12, no. 8, pp. 2038–2042, Aug. 1997.

[45] Z. Jing, M. O. Bloomfield, L. Jian-Qiang, R. J. Gutmann, and T. S. Cale, "Modeling thermal stresses in 3-D IC interwafer interconnects," *IEEE Trans. Semicond. Manuf.*, vol. 19, no. 4, pp. 437–448, Nov. 2006.

[46] D. R. Fridline and A. F. Bower, "Influence of anisotropic surface diffusivity on electromigration induced void migration and evolution," *J. Appl. Phys.*, vol. 85, no. 6, pp. 3168–3174, Mar. 1999.

[47] H. Ceric and S. Selberherr, "An adaptive grid approach for the simulation of electromigration induced void migration," *IEICE Trans. Electron.*, vol. E86-C, no. 3, pp. 421–426, 2002.

[48] D. N. Bhate, A. F. Bower, and A. Kumar, "A phase field model for failure in interconnect lines due to coupled diffusion mechanisms," *J. Mech. Phys. Solids*, vol. 50, no. 10, pp. 2057–2083, Oct. 2002.

[49] A. V. Vairagar, S. G. Mhaisalkar, A. Krishnamoorthy, and K. N. Tu, "In Situ observation of electromigration-induced void migration in dual-damascene Cu interconnect structures," *J. Appl. Phys.*, vol. 85, no. 13, pp. 2502–2504, Sep. 2004.

[50] E. Zschech and V. Sukharev, "Microstructure effect on EM-induced copper interconnect degradation," *Microelectron. Eng.*, vol. 82, no. 3/4, pp. 629–638, Dec. 2005.

[51] R. Rosenberg and M. Ohring, "Void formation and growth during electromigration in thin films," *J. Appl. Phys.*, vol. 42, no. 13, pp. 5671–5679, Dec. 1971.

[52] V. Sukharev, E. Zschech, and W. D. Nix, "A model for electromigration-induced degradation mechanisms in dual-inlaid copper interconnects: Effect of microstructure," *J. Appl. Phys.*, vol. 102, no. 5, p. 053 505, Sep. 2007.

Hajdin Ceric was born in Sarajevo, Bosnia and Herzegovina, in 1970. He received the B.S. degree in electrical engineering from the University of Sarajevo, Sarajevo, and the Diplomingenieur degree and the Ph.D. degree in technical sciences from the Technische Universität Wien, Vienna, Austria, in 2000 and 2005, respectively.

In June 2000, he joined the Institut für Mikroelektronik, Technische Universität Wien, where he is currently a Postdoctoral Researcher. His scientific interests include interconnect and process simulation.

Roberto Lacerda de Orio was born in Sao Paulo, Brazil, in 1981. He received the M.S. degree in electrical engineering from the State University of Campinas, Campinas, in 2006. He is currently working toward the Ph.D. degree at the Institut für Mikroelektronik, Technische Universität Wien, Vienna, Austria.

In September 2006, he joined the Institut für Mikroelektronik, Technische Universität Wien. His scientific interests include electromigration modeling and simulation.

Johann Cervenka was born in Schwarzach, Austria, in 1968. He received the Diplomingenieur degree in electrical engineering and the Ph.D. degree in technical sciences from the Technische Universität Wien, Vienna, Austria, in 1999 and 2004, respectively.

In November 1999, he joined the Institut für Mikroelektronik, Technische Universität Wien. His scientific interests include 3-D mesh generation, as well as algorithms and data structures in computational geometry.

Siegfried Selberherr (M'79–SM'84–F'93) was born in Klosterneuburg, Austria, in 1955. He received the M.S. degree in electrical engineering and the Ph.D. degree in technical sciences from Technische Universität Wien, Wien, Austria, in 1978 and 1981, respectively.

Since 1984, he has been holding the "venia docendi" on computer-aided design. Since 1988, he has been the Chair Professor of the Institut für Mikroelektronik, Technische Universität Wien. From 1998 to 2005, he was the Dean of the Fakultät für Elektrotechnik und Informationstechnik. His current research interests are modeling and simulation of problems for microelectronics engineering.